New Journal of Physics
The open access journal at the forefront of physics

Deutsche Physikalische Gesellschaft DPG
IOP Institute of Physics

Published in partnership with: Deutsche Physikalische Gesellschaft and the Institute of Physics

OPEN ACCESS

RECEIVED
6 August 2021

REVISED
15 October 2021

ACCEPTED FOR PUBLICATION
3 November 2021

PUBLISHED
25 November 2021

PAPER

Theoretical aspects of radium-containing molecules amenable to assembly from laser-cooled atoms for new physics searches

Timo Fleig[1,*] and David DeMille[2]

[1] Laboratoire de Chimie et Physique Quantiques, FeRMI, Université Paul Sabatier Toulouse III, 118 Route de Narbonne, F-31062 Toulouse, France
[2] Department of Physics, University of Chicago, Chicago, IL 60637, United States of America
[*] Author to whom any correspondence should be addressed.

E-mail: timo.fleig@irsamc.ups-tlse.fr and ddemille@uchicago.edu

Keywords: electron electric dipole moment, *P*, *T* symmetry violation, relativistic electronic structure, ultracold molecules, laser-coolable atoms

Abstract

We explore the possibilities for a next-generation electron-electric-dipole-moment experiment using ultracold heteronuclear diatomic molecules assembled from a combination of radium and another laser-coolable atom. In particular, we calculate their ground state structure and their sensitivity to parity- and time-reversal ($\mathcal{P},\mathcal{T}$) violating physics arising from flavor-diagonal charge-parity ($\mathcal{CP}$) violation. Among these species, the largest $\mathcal{P},\mathcal{T}$-violating molecular interaction constants—associated for example with the electron electric dipole moment—are obtained for the combination of radium (Ra) and silver (Ag) atoms. A mechanism for explaining this finding is proposed. We go on to discuss the prospects for an electron EDM search using ultracold, assembled, optically trapped RaAg molecules, and argue that this system is particularly promising for rapid future progress in the search for new sources of $\mathcal{CP}$ violation.

1. Introduction

The detection of a charge-parity ($\mathcal{CP}$) violating signal of leptonic or semi-leptonic origin would open a route [1, 2] for explaining so far not understood aspects of the observed matter and energy content of the Universe, in particular its matter–antimatter dissymmetry [3]. Under the assumption that $\mathcal{CPT}$ invariance ($\mathcal{T}$ denoting time reversal) of fundamental physical laws holds [4], the detection of an electric dipole moment (EDM) along the angular momentum of any system would reveal the influence of $\mathcal{CP}$-violating interactions. EDMs are very insensitive to the $\mathcal{CP}$-odd phases already incorporated into the standard model (SM) of elementary particles (via flavor mixing matrices), so EDMs act as very low-background signals for beyond SM $\mathcal{CP}$-odd interactions [5, 6]. For this reason, atomic and molecular searches for flavor-diagonal violations of $\mathcal{CP}$ symmetry [7] have become a field of intense research at the forefront of new physics searches [8–10]. In this paper, we focus on $\mathcal{P},\mathcal{T}$-violating effects that explicitly couple to electron spin—in particular, the electron EDM, nucleon–electron scalar–pseudoscalar (Ne-SPS) coupling, and nuclear magnetic quadrupole moment (NMQM). The sensitivity of a given atomic or molecular species to these effects can be parameterized in terms of the associated $\mathcal{P},\mathcal{T}$-violating interaction constants: the effective internal field acting on the electron EDM, E_{eff}; the Ne-SPS interaction constant W_S; and the NMQM interaction constant W_M. We refer to the entire set of these interaction constants as 'the $\mathcal{P},\mathcal{T}$-odd constants'.

Among various future directions considered to search for $\mathcal{P},\mathcal{T}$-odd effects coupled to the electron spin with greater sensitivity [11], experiments based on ultracold and optically trapped molecules [12, 13] appear particularly promising [10, 14, 15]. Here, the structure of polar molecules amplifies the observable energy shifts due to underlying mechanisms for $\mathcal{CP}$ violation [16, 17]. Optical trapping could provide long spin coherence times [18–20] for large molecular ensembles [21], and hence unprecedented energy resolution. With plausible projected values of experimental parameters, this could provide ∼3 orders of magnitude improved statistical sensitivity relative to the current state of the art for the $\mathcal{P},\mathcal{T}$-odd constants

of interest here [15]. There are significant advantages in using molecules at the lowest possible temperatures, i.e. near the regime of quantum degeneracy. Here, possible systematic errors due to the trapping light can be minimized by using weak, low-intensity trapping light [22, 23]. Moreover, the high and deterministic densities typical of lattice-trapped quantum gases [24] open the potential to employ spin-squeezing methods to surpass the standard quantum limit of statistical sensitivity [25] (which is already typically reached in EDM experiments, and assumed in the estimate above). In principle, squeezing could enable sensitivity improved by up to another ∼1–3 orders of magnitude [25–27].

Implementing this vision requires identifying suitable molecular species—that is, species with large values of the $\mathcal{P},\mathcal{T}$-odd constants, and which also plausibly can be trapped and cooled to near the regime of quantum degeneracy. To date, discussion of potential species with these properties has centered on paramagnetic molecules with structure suitable for direct laser cooling, such as YbF or YbOH or RaF [14, 15, 28, 29]. However, the coldest and densest molecular gases to date have been produced not by direct laser cooling, but instead by assembly of diatomic species from pairs of ultracold atoms [21, 30]. An early investigation of the prospects for EDM experiments with such systems was made by Meyer *et al* [31]. They considered the neutral species RbYb and CsYb, which have the unpaired electron needed for high sensitivity to the electron EDM and which could be assembled from atoms routinely cooled to quantum degeneracy. However, they found that the values of $E_{\rm eff}$ in these molecules were much smaller than expected from simple scaling arguments—in each case, $E_{\rm eff} < 1$ GV cm^{-1}. This is roughly two orders of magnitude smaller than $E_{\rm eff}$ in ThO, the species used by the ACME experiment to place the best current limit on the electron EDM [32]. To our knowledge, the idea to use 'assembled' ultracold molecules for EDM experiments has since not been discussed further in the literature.

A suitable molecular species to be assembled and used to measure the electron EDM must satisfy several criteria. Naturally, both constituent atoms must be amenable to laser cooling and trapping. For large values of the $\mathcal{P},\mathcal{T}$-odd constants of interest here, the molecule must have an unpaired electron spin in its absolute ground state. These two criteria together suggest using molecules where one atom has alkali-like structure (single unpaired electron), and the other has alkaline earth-like structure (closed electron shell). Because the values of the $\mathcal{P},\mathcal{T}$-odd constants scale roughly as Z^3 (where Z is the atomic number) [33–35], at least one of the atoms should be very heavy to maximize their values. Though less critical, it is experimentally convenient to use species that can be strongly polarized in small electric fields; this can be enabled by a large molecular dipole moment and/or small molecular rotational splitting [36].

In 2018, the present authors presented the RaAg molecule [37] as a very promising ultracold molecular system for electron EDM searches. Use of the alkaline earth atom radium (Ra) as the required heavy nucleus for such a future experiment is strongly suggested, since Ra ($Z = 88$) is the heaviest atom where laser cooling and trapping has been demonstrated [38]. The choice of the silver (Ag) atom rather than a true alkali atom as the bonding partner for Ra is less obvious. However, the coinage metals (Cu, Ag, Au) have a nominally alkali-like structure, with one valence *s* electron above closed shells, so they are in principle amenable to laser cooling. Indeed, laser cooling and trapping of Ag atoms was demonstrated already over 20 years ago [39]. In addition, the coinage metals (CMs) have much larger electron affinities (EA) [40, 41] than the alkalis. Hence, we anticipated that they might form a strong polar bond with the highly polarizable Ra atom [42, 43]. This type of bond is generically correlated both with a large effective electric field on the electron EDM [35, 44], and with a large molecular dipole moment. Large molecular dipole moments in Ra-CM molecules, discussed here, have also been found in references [36, 45]. Sunaga *et al* [36] discussed properties of radium-A molecules—where A is a halogen or a coinage-metal atom—relevant to molecular electron EDM searches. A more encompassing view on the possibilities of using ultracold diatomic molecules assembled from laser-coolable atoms, however, was not discussed in that paper. Here, we present a comparative study of the effective electric field $E_{\rm eff}$ acting on the electron EDM in radium-X molecules, where X is a (potentially) laser-coolable alkali or CM atom.

The following section summarizes the theory underlying the presented results on molecular structure. Section 3 contains a comparative study of a systematic series of Ra-alkali and Ra-coinage-metal diatomics with an emphasis on $\mathcal{P},\mathcal{T}$-odd and spectroscopic properties. In the final section we conclude, mention ongoing work [46], and lay out some prospects for the very near future.

2. Theory

2.1. General definitions and wavefunctions

The electronic many-body states of all of the present molecules are denoted as $|\Omega\rangle$ with $\Omega = |M_J|$. These states are represented by relativistic configuration interaction wavefunctions

$$|\Omega\rangle \equiv \sum_{I=1}^{\dim\ \mathcal{F}^t(M,n)} c_{(\Omega),I}(\mathcal{S}\overline{\mathcal{T}})_I|\quad\rangle, \tag{1}$$

where $\mathcal{F}^t(M,n)$ is the symmetry-restricted sector of Fock space with n electrons in M four-spinors, $\mathcal{S} = a_i^\dagger a_j^\dagger a_k^\dagger \ldots$ is a string of spinor creation operators, $\overline{\mathcal{T}} = a_{\overline{l}}^\dagger a_{\overline{m}}^\dagger a_{\overline{n}}^\dagger \ldots$ is a string of creation operators of time-reversal transformed spinors. The determinant expansion coefficients $c_{(\Omega),I}$ are generally obtained as described in references [47, 48] by diagonalizing the Dirac–Coulomb Hamiltonian, in a.u.

$$\hat{H}^{\text{Dirac–Coulomb}} = \sum_j^n \left[c\,\boldsymbol{\alpha}_j \cdot \mathbf{p}_j + \beta_j c^2 - \frac{Z}{r_j}\mathbb{1}_4\right] + \sum_{j,k>j}^n \frac{1}{r_{jk}}\mathbb{1}_4 \tag{2}$$

in the basis of the states $(\mathcal{S}\overline{\mathcal{T}})_I\,|\quad\rangle$, where the indices j, k run over electrons, Z is the proton number, and $\boldsymbol{\alpha}, \beta$ are standard Dirac matrices. The specific models used in the present work will be discussed in subsection 3.1.2. The calculation of properties using the resulting CI eigenvectors is technically carried out as documented in references [49, 50]. Atoms and linear molecules are treated in a finite sub-double group of $D_{\infty h}^*$ (atoms) or $C_{\infty v}^*$ (heteronuclear diatomic molecules) which gives rise to a real-valued formalism in either case [51]. Definitions of the various property operators used in the present work will be given in the following sections.

2.2. $\mathcal{P},\mathcal{T}$-odd properties

The electron EDM interaction constant is evaluated as proposed in stratagem II of Lindroth *et al* [52] as an effective one-electron operator via the squared electronic momentum operator. In the present work $\mathcal{P},\mathcal{T}$-violating properties are only calculated in molecules so with zeroth-order states denoted as $|\Omega\rangle$

$$E_{\text{eff}} = \frac{2\imath c}{e\hbar}\,\langle\Omega|\sum_{j=1}^n \gamma_j^0\gamma_j^5 \mathbf{p}_j^{\,2}\,|\Omega\rangle \tag{3}$$

with n the number of electrons and j an electron index. The implementation in the many-body framework is described in greater detail in reference [53]. The EDM effective electric field is related to the electron EDM interaction constant $W_d = -\frac{1}{\Omega}E_{\text{eff}}$.

A measurement on open-shell molecules also tests C_S, the fundamental Ne-SPS coupling constant for a neutral weak current between electrons and nucleons [54]. In the framework of an effective field theory the Ne-SPS interaction energy [35] can be written as

$$\varepsilon_{\text{Ne–SPS}} = W_S\,C_S, \tag{4}$$

where

$$W_S := \frac{\imath}{\Omega}\frac{G_{\text{F}}}{\sqrt{2}}A\,\langle\Omega|\sum_{j=1}^n \gamma_j^0\gamma_j^5\,\rho(\mathbf{r}_j)\,|\Omega\rangle \tag{5}$$

is the Ne-SPS interaction constant for the nucleus with A nucleons, G_{F} is the Fermi constant, γ is an electronic Dirac matrix, and $\rho(\mathbf{r})$ is the nuclear density at position $\mathbf{r}$. The implementation in the molecular framework is documented in reference [55].

The nuclear magnetic quadrupole moment interaction constant has been implemented in reference [56] and can be written as

$$W_M = \frac{3}{2\Omega}\,\langle\Omega| - \frac{1}{3}\sum_{j=1}^n \left\{\left[\alpha_1(j)\frac{\partial}{\partial r_2(j)} - \alpha_2(j)\frac{\partial}{\partial r_1(j)}\right]\frac{r_3(j)}{r^3(j)}\right\}|\Omega\rangle\,. \tag{6}$$

In this case, $r_k(j)$ denotes the kth Cartesian component of vector $\mathbf{r}$ for particle j (*idem* for the Dirac matrices $\boldsymbol{\alpha}$).

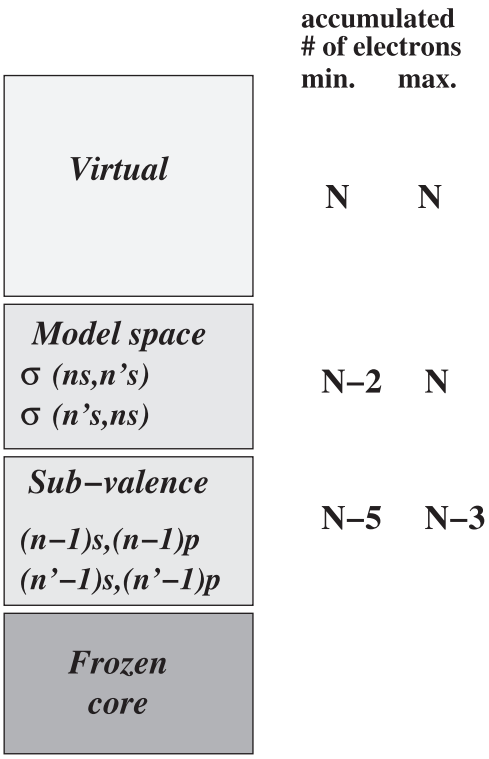

Figure 1. Wavefunction definitions for alkali-radium diatomic molecules. Up to two holes are allowed in the sub-valence spinors which accounts for correlation effects among the sub-valence electrons and with the valence electrons. The model space is restricted to the valence spinors where all occupations are allowed. The cutoff for the virtual space is set to 10 [a.u.].

2.3. Other properties

The rotational constant is defined for a classical rigid rotor as $B = \frac{\hbar^2}{2I}$ with $I = \mu R$ the moment of inertia in terms of the reduced mass μ and the internuclear distance R. Thus, in units of inverse length,

$$B_e = \frac{B}{hc} = \frac{\hbar}{4\pi c \mu R_e^2}. \tag{7}$$

R_e is in the present obtained from quantum-mechanical calculations.

3. Results

3.1. Computational details

3.1.1. Basis sets and molecular spinors

Uncontracted Gaussian atomic basis sets have been used for all considered systems: for Ra Dyall's triple-ζ set [57, 59] including outer-core correlating functions, amounting to {33*s*, 29*p*, 18*d*, 12*f*, 3*g*, 1*h*}; for Li and Na the EMSL aug-cc-pVTZ sets [60]; for K, Rb, Cs and Fr Dyall's TZ bases including $(n-1)s, (n-1)p, ns$-correlating functions (also $(n-2)d$-correlating for Cs and Fr) [57].

Molecular spinors are obtained from Dirac–Coulomb Hartree–Fock (DCHF) calculations using the DIRAC program package [51] in a locally modified version. Since the present systems have an odd total number of electrons fractional occupation is used for defining the Fock operator: $f = 0.5$ per spinor for one Kramers pair and the open-shell spinor pair is a molecular superposition of radium-alkali (RaA) atomic contributions. For Ra-coinage-metal (RaC) molecules the fractional occupation is $f = 0.75$ per spinor for the two Kramers pairs denoted σ and σ^* in figure 2.

3.1.2. Correlated wave functions

The generalized active space technique [61, 62] is ensuingly exploited for efficiently taking into account leading interelectron correlation effects. The model space generally includes all spinors required to describe the molecular ground state including leading electron correlation effects.

For the RaA calculations a specific model is adopted that allows for an economic description of the molecular ground state including electron-correlation effects. Figure 1 shows how the wavefunction is linearly parameterized for this set of calculations.

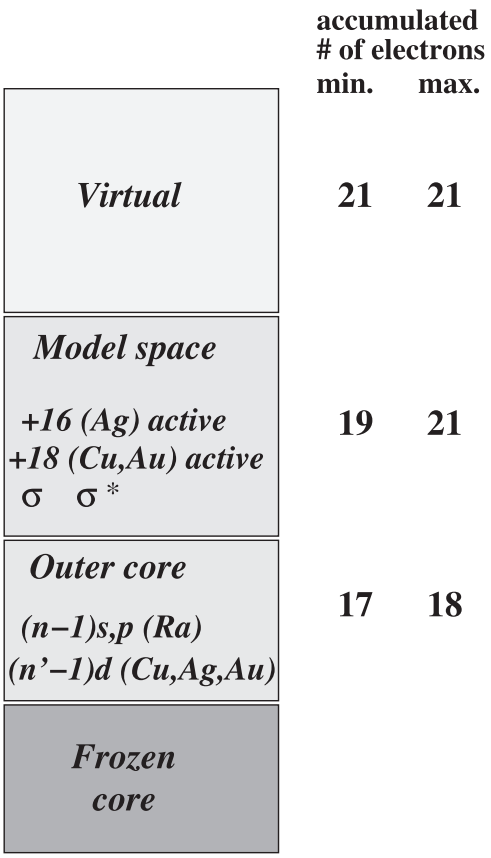

Figure 2. Wavefunction definitions for coinage-metal-radium diatomic molecules. Up to one hole is allowed in the outer-core spinors which accounts for core-valence correlations between those electrons and the respective valence electrons. In the model space all occupations within the given constraints are allowed. σ is a molecular spinor pair with predominantly Cu 4*s*/Ag 5*s*/Au 6*s* and some Ra 7*s* character. σ^* is a molecular spinor pair with predominantly Ra 7*s* and some Cu 4*s*/Ag 5*s*/Au 6*s* character. The cutoff for the virtual space is set to 5 [a.u.] (CuRa) and 4 [a.u.] (RaAg and RaAu).

For the RaC calculations a different model has been chosen which is shown in figure 2.

3.1.3. Rovibrational properties

Reduced masses are obtained for the most abundant isotopes ^{7}Li, ^{23}Na, ^{39}K, ^{85}Rb, ^{133}Cs, ^{223}Fr, ^{107}Ag, and ^{226}Ra with data taken from reference [63].

3.2. Alkali- and coinage-metal-radium molecules

3.2.1. Trends

The purpose of this section is to show trends for properties of interest among diatomic molecules that are candidates for measurement of a $\mathcal{P},\mathcal{T}$-odd signal in the lepton sector. The interaction constants for their main sensitivity in this regard are compared for alkali (A) atoms and coinage-metal (C) atoms bound to atomic radium, see table 1. Among the A-Ra molecules the trends are consistent for E_{eff}, W_S, and W_M where in all cases the interaction constants increase monotonically with decreasing nuclear charge of A. These constants have been obtained at equilibrium internuclear separation R_e, along with other spectroscopic properties and the molecule-frame EDM D. It is worth noting that the root mean-square radii for the *ns* electron of the atoms A or C, here obtained from atomic quantum-mechanical calculations, are a good predictor of R_e, in the sense that the ratio $\frac{R_e\,(\mathrm{a.u.})}{\sqrt{\langle \hat{r}^2\rangle_{ns}}\,(\mathrm{a.u.})}$ is nearly constant across all the considered molecules. The greatest deviations from the mean value of this ratio amount to around 7% for Na (upper end) and Ag (lower end).

Since analytical relationships between the matrix elements of $\mathcal{P},\mathcal{T}$-odd interactions exist [64] and these relationships have also been corroborated in numerical studies of various complex systems [65, 66] the trends for these interactions are expected to be very similar which is confirmed by the results in table 1. The principal mechanism explaining this trend becomes obvious when considering the EA of A. A free Ra atom has no unpaired electrons and a $^{1}S_0(7s^2)$ ground state insensitive to the present $\mathcal{P},\mathcal{T}$-odd interactions. In the molecular environment, however, the partner atom A will draw electron density from Ra leading to

Table 1. Equilibrium internuclear distances R_e, harmonic vibrational frequencies ω_e, rotational constants B_e, molecule-frame static EDM D, polarizing external field $E_{pol} = \frac{2B_e}{D}$, electron EDM effective electric field E_{eff}, Ne-SPS interaction constants W_S, and nuclear magnetic-quadrupole moment interactions constants W_M for the electronic ground states $^2\Sigma_{1/2}$ of diatomics RaA and RaC; for RaLi two sets of results are shown using two different cutoff energies for the virtual spinor set; experimental EA and root mean-square radius for the valence s electron spinor $\sqrt{\langle \hat{r}^2 \rangle_{ns}}$ in a.u. for alkali and coinage-metal atoms. $\mathcal{P},\mathcal{T}$-odd constants are evaluated at the respective R_e.

	R_e (a.u.)	ω_e (cm^{-1})	B_e (cm^{-1})	D (Debye)	$\sqrt{\langle \hat{r}^2 \rangle_{ns}}$	EA (eV)	E_{eff} (GV cm^{-1})	W_S (kHz)	W_M ($\frac{10^{33}\ \text{Hz}}{e\ \text{cm}^2}$)	E_{pol} (kV cm^{-1})
RaLi(10 a.u.)	7.668	105.4	0.151	1.36	4.21	0.618 [67]	22.2	−59.5	0.652	13.3
RaLi(50 a.u.)	7.689	103.8	0.150	1.34	4.21	0.618 [67]	21.7	−58.3	0.641	13.3
RaNa	8.703	39.3	0.038	0.51	4.54	0.548 [68]	12.0	−32.2	0.368	8.90
RaK	10.37	20.7	0.017	0.39	5.60	0.501 [69]	5.44	−14.6	0.167	5.18
RaRb	10.75	14.5	0.008	0.36	5.93	0.486 [70]	5.01	−13.6	0.152	2.75
RaCs	11.25	12.0	0.006	0.46	6.48	0.472 [71]	4.52	−12.6	0.138	1.48
RaFr	11.26	10.5	0.004	0.24	6.31	0.486 [72]	3.44	−12.4	0.137	2.06
RaCu	6.050	106.7	0.033	4.30	3.54	1.236 [40]	67.0	−180.6	1.771	0.92
RaAg [37]	6.241	90.0	0.021	4.76	3.73	1.304 [40]	63.9	−175.1	1.761	0.53
RaAu	5.836	98.4	0.017	5.71	3.30	2.309 [41]	50.4	−166.4	1.752	0.36

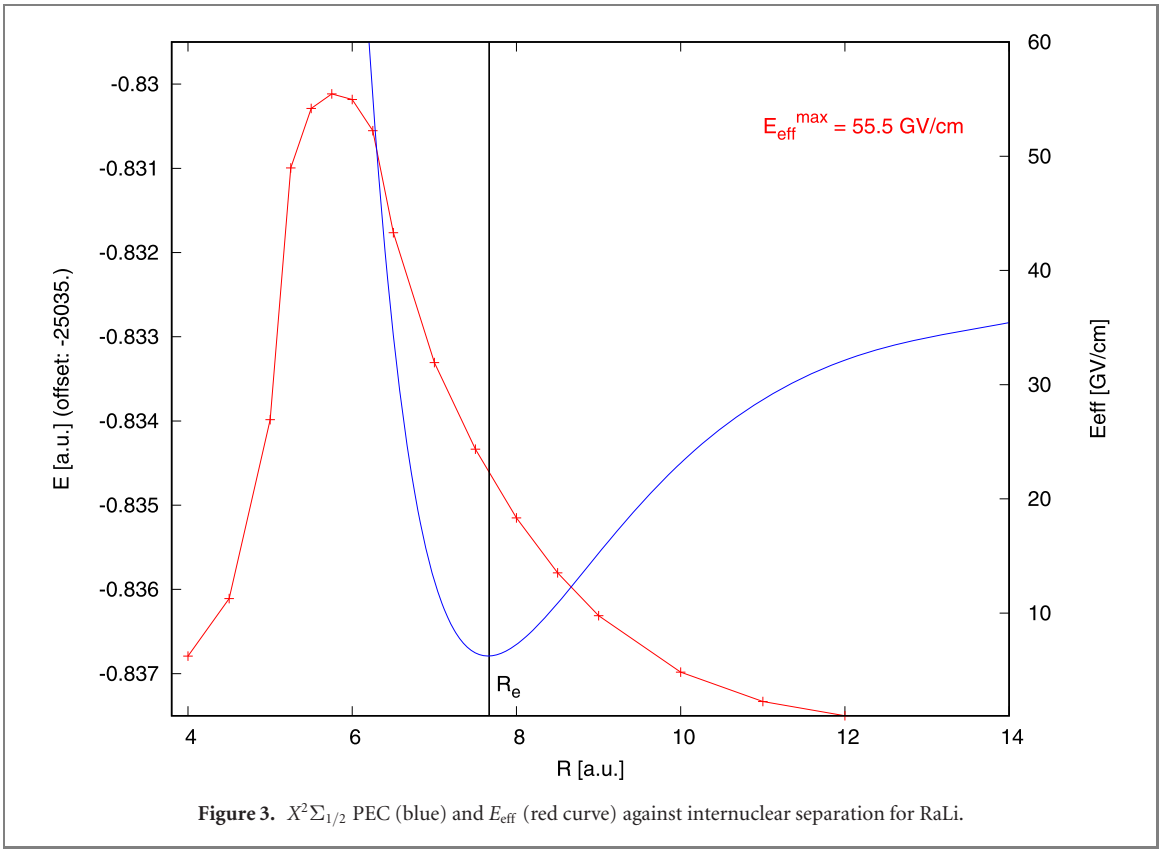

Figure 3. $X^2\Sigma_{1/2}$ PEC (blue) and E_{eff} (red curve) against internuclear separation for RaLi.

effective spin density on the latter. This effect is a function of EA(A) and manifests itself in non-zero $\mathcal{P},\mathcal{T}$-odd interactions.

This mechanism of creating spin density on Ra is qualitatively the same for all Ra-A combinations. However, there exist pronounced quantitative differences for the different partner atoms A, leading to sizeable differences in E_{eff} at the equilibrium internuclear separation of the respective molecule. Figure 3 shows that E_{eff} goes through a maximum at separations shorter than R_e for RaLi and drops off quite sharply as the molecule is stretched beyond R_e. The corresponding situation for RaAg is displayed in figure 4. In contrast to RaLi the RaAg curve for E_{eff} hardly drops off from the maximum value as R passes through the minimum of the potential-energy curve (PEC) but instead displays a shoulder that extends to values $R > R_e$. Even though $E_{eff\ max}$(RaAg) ≈ 70 GV cm^{-1} is only about 25% greater than $E_{eff\ max}$(RaLi) ≈ 56 GV cm^{-1}, the shoulder leads to almost a factor of 3 difference between E_{eff}(RaAg) and E_{eff}(RaLi) at the respective values of R_e.

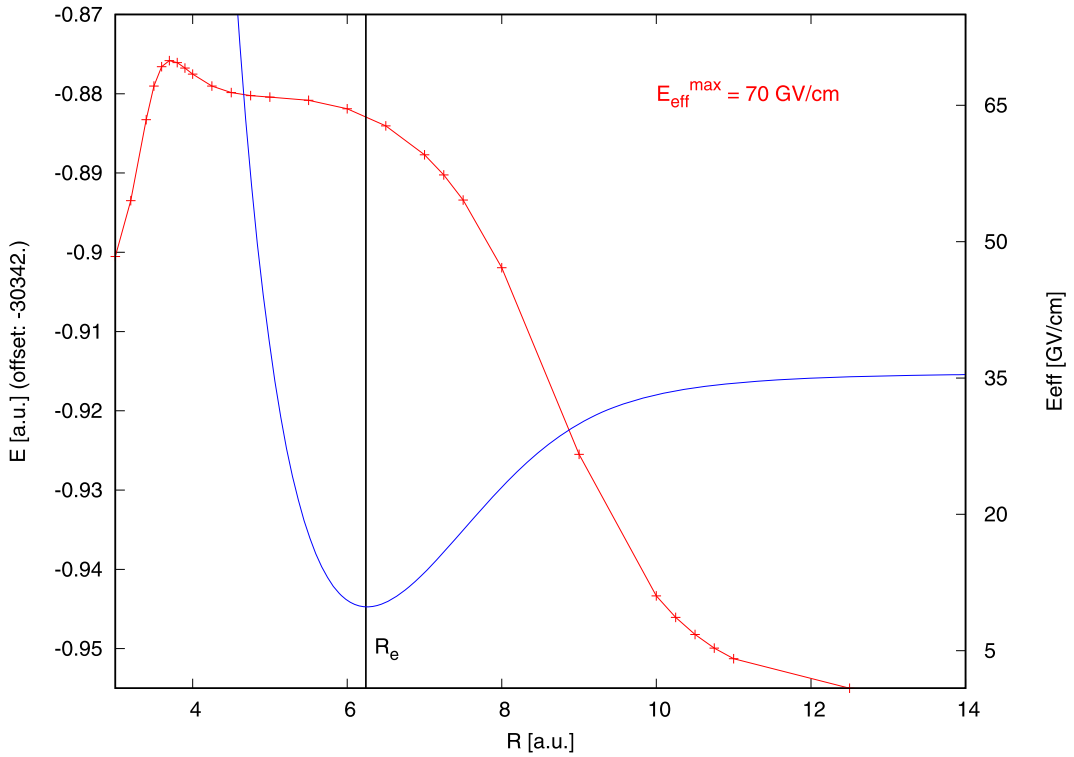

Figure 4. $X^2\Sigma_{1/2}$ PEC (blue) and $E_{\rm eff}$ (red curve) against internuclear separation for RaAg.

With the present electronic-structure models we find $R_{E_{\rm eff\,max}} = 5.75$ a.u. and $R_{\rm e} = 7.69$ a.u. for RaLi. The change of molecule-frame EDM between these two points is $\Delta D = D(R_{\rm e}) - D(R_{E_{\rm eff\,max}}) = 0.84$ Debye, and the full dipole-moment curve is shown in figure 5. This is a positive but rather modest value. On the contrary, for RaAg $R_{E_{\rm eff\,max}} = 3.7$ a.u., $R_{\rm e} = 6.24$ a.u. and $\Delta D = D(R_{\rm e}) - D(R_{E_{\rm eff\,max}}) = 1.8$ Debye, as shown in figure 6. In addition to the EDM being much greater at $R_{\rm e}$ in RaAg, it also displays a sharper increase between the two significant points, indicating that the partial charge remains on the Ag atom even when the internuclear distance is stretched slightly beyond $R_{\rm e}$. This leads to a shoulder both for the spin density on the Ra atom and $E_{\rm eff}$ in RaAg. The underlying principal explanation is, therefore, strongly suggested to indeed be the electron affinity of the atom polarizing the heavy target atom (Ra).

A further analysis shows that the partial charge $\delta_{\rm A}^-$ on the atom A at $R_{\rm e}$ calculated from DCHF valence s spinors increases (on the absolute) from $\delta_{\rm Fr}^- \approx -0.03e$ to $\delta_{\rm Rb}^- \approx -0.05e$ to $\delta_{\rm Li}^- \approx -0.08e$ and reaches $\delta_{\rm Ag}^- \approx -0.24e$ in RaAg, leading to a significantly greater $E_{\rm eff}$ in RaAg than in RaLi.

Turning to a comparison of the coinage-metal-Ra molecules it becomes clear that the above analysis in terms of EA alone is not sufficient for explaining all trends. Au has a much greater EA than Cu or Ag but still yields a smaller $E_{\rm eff}$ when bound to Ra. The maximum value for $E_{\rm eff}$ as a function of R is greatest for CuRa which also displays the characteristic shoulder as discussed above for the case of RaAg (although it is less pronounced in RaCu). In the case of RaAu, the shoulder is significantly less pronounced than in RaAg in addition to the maximum $E_{\rm eff}(R)$ being smallest among all coinage-metal-Ra molecules. An explanation for this observation in terms of s–p-mixing matrix elements and relevant spinor energies has been attempted in reference [36]. We refrain from delving into a deeper analysis of the related trends for $E_{\rm eff}(R)$ in coinage-metal-Ra molecules since, as explained below, neither Cu nor Au atoms have significant advantages, relative to Ag, for use in an ultracold assembled molecule EDM experiment.

We also consider a further important aspect for experimental feasibility: the external electric field $E_{\rm pol} = 2B_{\rm e}/D$ required for fully polarizing the molecule. The comparison in table 1 demonstrates that RaAg is among the best of the laser-coolable atom combinations also in this respect (surpassed only by RaAu, by a factor of only 1.5). The extremely small $E_{\rm pol}$ required for RaAg is due to its much greater molecule-frame EDM—about an order of magnitude—as compared with heavier alkali-radium molecules. This by far outweighs the slight disadvantage RaAg has in terms of its rotational constant $B_{\rm e}$, which is roughly

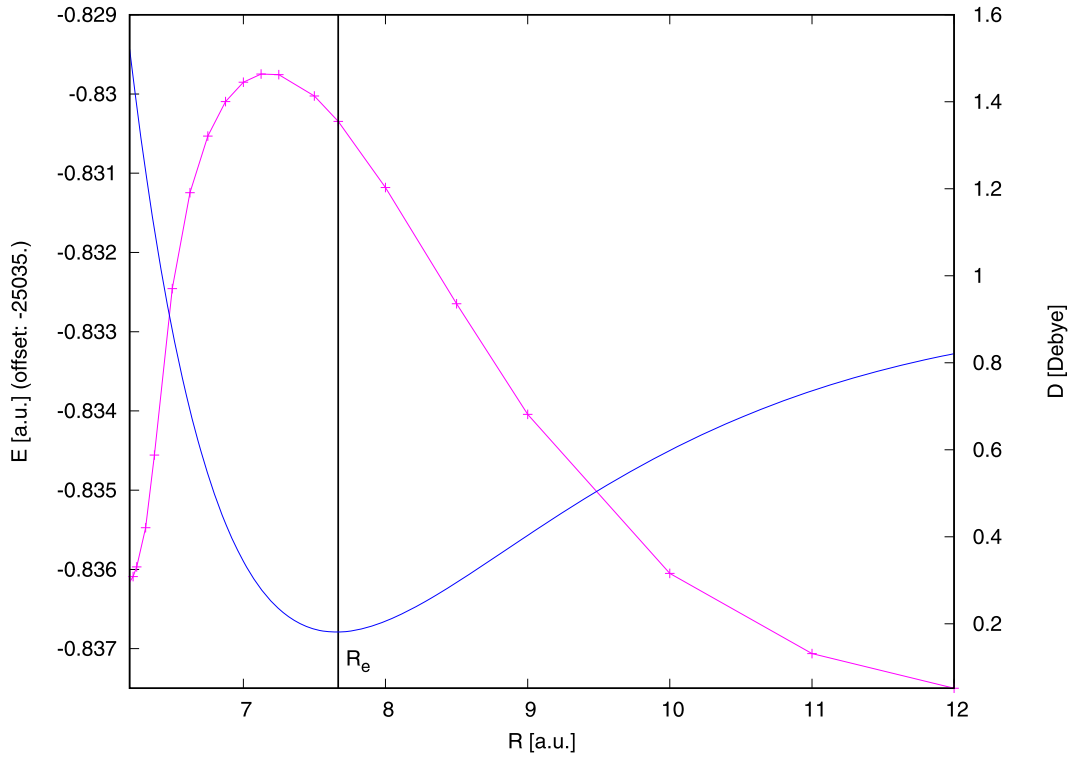

Figure 5. $X^2\Sigma_{1/2}$ PEC (blue) and molecule-frame EDM D (magenta curve) against internuclear separation for RaLi (cutoff 10 a.u.).

a factor of three greater than B_e for RaCs, as an example. A similar conclusion was reached in references [36, 45].

3.2.2. Comparison of models and with the literature

The studies in the previous section have a focus on establishing trends and explaining qualitatively important features of the candidate set of molecules. For RaAg the corresponding wavefunction model is defined in figure 2 and we will here call it TZ/MR-CISD. Models of similar quality have been used for the other molecules in this work for the mentioned purposes.

In the following we compare the TZ/MR-CISD to a more accurate model QZ/MR-CISDT which differs from the previous one in two ways: QZ/MR-CISDT uses Gaussian basis sets of quadruple-zeta (QZ) quality [57, 58] for both Ra and Ag atoms. Second, the model space now only consists of the Kramers pairs σ and σ^*, but in turn the highest particle rank of the virtual spinor space has been increased from 2 to 3. The model QZ/MR-CISDT is, therefore, significantly more accurate than the model TZ/MR-CISD for a calculation of the electronic ground state.

Comparative results are shown in table 2. The results for our spectroscopic and $\mathcal{P},\mathcal{T}$-odd constants for RaAg from the two presented models differ by less than 5%, except for ω_e where the difference is around 9%. The results from our more accurate model, QZ/MR-CISDT, differ from those of Śmiałkowski *et al* by less than 4%. The results presented in reference [45] have been obtained with large valence atomic basis sets and a high-quality wavefunction model and are certainly the more reliable values for comparison than those obtained by Sunaga *et al* [36] where basis sets of only double-zeta (DZ) quality have been used. However, Śmiałkowski *et al* use effective core potentials (ECP) whereas our calculations employ Dirac wavefunctions for the entire set of atomic shells.

Concerning the difference of E_{eff} with the result from reference [36] we tested a basis set of DZ quality [57, 58] and obtain $E_{\mathrm{eff}}(R = 6.0\ \mathrm{a.u.}) \approx 72\ \mathrm{GV\,cm^{-1}}$ at an internuclear separation close to R_e determined in the work of Sunaga *et al* which is very close to the result from reference [36] in table 2. Since the two employed wavefunction models (MR-CISDT and CCSD) are similar in quality this demonstrates that the use of too small a basis set will lead to a significant overestimation of E_{eff} for RaAg. W_S in reference [36] is, therefore, also too large on the absolute. It is clear, however, that reference [36] did not aim at highly accurate results but rather at determining trends for a set of molecules.

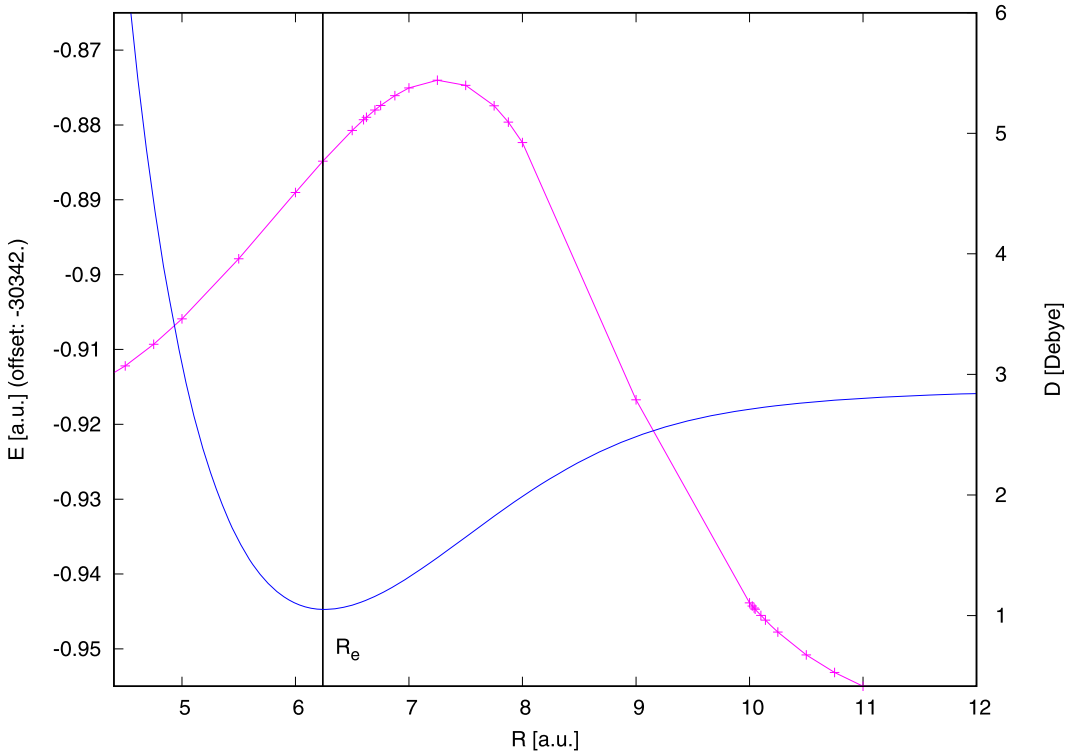

Figure 6. $X^2\Sigma_{1/2}$ PEC (blue) and molecule-frame EDM D (magenta curve) against internuclear separation for RaAg.

Table 2. Spectroscopic and $\mathcal{P},\mathcal{T}$-odd constants for RaAg.

Source	R_e (a.u.)	ω_e (cm^{-1})	B_e (cm^{-1})	D (Debye)	$E_{\rm eff}$ (GV cm^{-1})	W_S (kHz)	W_M ($\frac{10^{33}\ \rm Hz}{e\ \rm cm^2}$)	$E_{\rm pol}$ (kV cm^{-1})
Present TZ/MR-CISD [37]	6.241	90.0	0.0213	4.76	63.9	−175.1	1.761	0.53
Present TZ/MR-CISD [37]	6.128	98.2	0.0221	4.89	66.1	−181.1	1.821	0.54
Śmiałkowski *et al* [45] CCSD(T)	5.959	100.6	0.0234	5.08				0.55
Sunaga *et al* [36] CCSD	6.10		0.022	5.1	73.7	−201.8		0.52

4. Conclusions and outlook

In the present work we have shown that radium-CM molecules have much greater $\mathcal{P},\mathcal{T}$-odd interaction constants than Ra-alkali molecules, which are the natural species to consider for assembly from ultracold atoms and high sensitivity to the electron EDM. Moreover, a simple explanation was developed for how these effects reach near-optimal values in Ra-CM molecules. We also showed that these RaC species have large intrinsic molecule-frame dipole moments, which make them easily polarized using an external electric field of very modest strength.

From this perspective alone, any of the Ra-CM molecules could be an interesting experimental system for future EDM experiments. However, let us return to the original goal, which was to find suitable species that can be assembled from ultracold atoms. Among the CMs, Ag turns out to be uniquely easy to laser cool and trap. In all the CM atoms, the last filled electron shell contains *d* orbitals, and the energy to excite one electron from the closed *d*-shell to the unfilled *s* orbital is quite comparable to that needed to excite the valence electron from its *ns* state to an *np* orbital (as desired for laser cooling). In both Cu and Au, the lowest *d*-shell excited states lie at least ∼2 eV below the *np* valence excited state, and the *np* state decays with significant branching ratio into these metastable levels [73]. Hence, laser cooling of Cu and Au would require additional laser(s) to repump the lower states, in addition to the primary laser driving the *ns*–*np* optical cycling transition [74]. This in turn would create a 'type-II' level structure, where the unavoidable presence of dark states significantly reduces the strength of optical forces [75]. By contrast, in the Ag atom the *d*-shell excited state is less than 0.025 eV below the $p_{3/2}$ valence excited state, and the branching ratio for

decay into the metastable state is effectively negligible [39]. Hence, in Ag a single laser is sufficient to produce maximal trapping and cooling forces, in complete analogy to standard alkali atoms [39]. For this reason, within the CM group only Ag has been cooled and trapped, and (to our knowledge) laser cooling of Au or Cu has not even been attempted. Since the values of the $\mathcal{P},\mathcal{T}$-odd interaction constants are no better in RaAu or RaCu than in RaAg, and the electric field needed to polarize RaAg is small enough to be experimentally convenient, we conclude that, among the considered species, RaAg is by far the most favorable for experiments of the considered type.

This leads to further questions about experimental viability of an electron EDM search using ultracold, assembled RaAg molecules. To date, no ultracold alkaline earth-alkali metal molecules of *any* species have been assembled. However, experimentally plausible pathways for such assembly have been identified for analogous species such as RbSr [76–78], YbLi [79], and YbCs [80], and considerable experimental progress has been made with each of these species [81–83]. Moreover, these pathways are based on extensive, successful experience with assembly of bi-alkali molecules [21]. For this reason, we consider it very plausible that RaAg molecules can, with sufficient effort, be assembled from ultracold Ra and Ag atoms.

All known and proposed techniques for ultracold molecule assembly rely on a two step, coherent process [12]. In the first step, atom pairs are transferred to a weakly-bound molecular state using either a Feshbach resonance [84] or near-threshold photoassociation [85, 86]. The weakly-bound state is then transferred to the rovibronic ground state, using stimulated Raman adiabatic passage (STIRAP) [87]. The relevant coupling strengths are determined by transition dipole moments between vibronic states for optical transitions [21], or by the structure of long-range bound states for Feshbach association [84]. To understand and reliably calculate all relevant coupling strengths, it is necessary to construct full PECs, including short-range and long-range internuclear parts, for ground and electronically excited molecular states. To address this question, we will in forthcoming work present predictions of the relevant features for RaAg. This will include dispersion coefficients for Ra and Ag atoms so far not established in the literature and required for the long-range parts of the relevant PECs, as well as calculations of short-range PECs and analysis of relevant vibronic transition dipole moments.

In summary: we have identified the radium-silver (RaAg) molecule as an exceptionally interesting system for a next-generation electron electric-dipole-moment experiment using ultracold, trapped molecules assembled from laser-coolable atoms. Further work is underway to evaluate details of the molecular structure that will determine the feasibility of Ra + Ag assembly with high efficiency.

Data availability statement

The data that support the findings of this study are available upon reasonable request from the authors.

ORCID iDs

Timo Fleig https://orcid.org/0000-0001-6002-2920

References

[1] Sakharov A D 1967 Violation of CP invariance, C asymmetry, and baryon asymmetry of the universe *JETP Lett.* **5** 24
[2] Cirigliano V, Ramsey-Musolf M J and van Kolck U 2013 Low energy probes of physics beyond the standard model *Prog. Part. Nucl. Phys.* **71** 2
[3] Dine M and Kusenko A 2003 Origin of the matter–antimatter asymmetry *Rev. Mod. Phys.* **76** 1
[4] Pauli W (ed) 1955 *Exclusion Principle, Lorentz Group and Reflection of Space-Time and Charge* (New York: McGraw-Hill) pp 30–51
[5] Pospelov M E and Khriplovich I B 1991 Electric dipole moment of the W boson and the electron in the Kobayashi–Maskawa model *Sov. J. Nucl. Phys.* **53** 638–40
Pospelov M E and Khriplovich I B 1991 *Yad. Fiz.* **53** 1030
[6] Yamaguchi Y and Yamanaka N 2021 Quark level and hadronic contributions to the electric dipole moment of charged leptons in the standard model *Phys. Rev.* D **103** 013001
[7] Raidal M *et al* 2008 Flavor physics of leptons and dipole moments *Eur. Phys. J.* C **57** 13
[8] Baron J *et al* 2014 Order of magnitude smaller limit on the electric dipole moment of the electron *Science* **343** 269
[9] Graner B, Chen Y, Lindahl E G and Heckel B R 2016 Reduced limit on the permanent electric dipole moment of ^{199}Hg *Phys. Rev. Lett.* **116** 161601
[10] Cairncross W B and Ye J 2019 Atoms and molecules in the search for time-reversal symmetry violation *Nat. Rev. Phys.* **1** 510
[11] Safronova M S, Budker D, DeMille D, Jackson Kimball D F, Derevianko A and Clark C W 2018 Search for new physics with atoms and molecules *Rev. Mod. Phys.* **90** 025008

[12] Carr L D, DeMille D, Krems R V and Ye J 2009 Cold and ultracold molecules: science, technology and applications *New J. Phys.* **11** 055049
[13] Bohn J L, Rey A M and Ye J 2017 Cold molecules: progress in quantum engineering of chemistry and quantum matter *Science* **357** 1002
[14] Fitch N J, Lim J, Hinds E A, Sauer B E and Tarbutt M R 2020 Methods for measuring the electron's electric dipole moment using ultracold YbF molecules *Quantum Sci. Technol.* **6** 014006
[15] Kozyryev I and Hutzler N R 2017 Precision measurement of time-reversal symmetry violation with laser-cooled polyatomic molecules *Phys. Rev. Lett.* **119** 133002
[16] Sandars P G H 1967 Measurability of the proton electric dipole moment *Phys. Rev. Lett.* **19** 1396
[17] Sushkov O P, Flambaum V V and Khriplovich I B 1984 Possibility of investigating *P*- and *T*-odd nuclear forces in atomic and molecular experiments *Sov. Phys. JETP* **60** 873
[18] Burchesky S, Anderegg L, Bao Y, Scarlett S Yu, Chae E, Ketterle W, Ni K-K and Doyle J M 2021 Rotational coherence times of polar molecules in optical tweezers (arXiv:2105.15199)
[19] Park J W, Yan Z Z, Loh H, Will S A and Zwierlein M W 2017 Second-scale nuclear spin coherence time of ultracold $^{23}Na^{40}K$ molecules *Science* **357** 372–5
[20] Gregory P D, Blackmore J A, Bromley S L, Hutson J M and Cornish S L 2021 Robust storage qubits in ultracold polar molecules (arXiv:2103.06310)
[21] Moses S A, Covey J P, Miecnikowski M T, Jin D S and Ye J 2017 New frontiers for quantum gases of polar molecules *Nat. Phys.* **13** 13
[22] Romalis M V and Fortson E N 1999 Zeeman frequency shifts in an optical dipole trap used to search for an electric-dipole moment *Phys. Rev.* A **59** 4547
[23] Chin C, Leiber V, Vuletić V, Kerman A J and Chu S 2001 Measurement of an electron's electric dipole moment using Cs atoms trapped in optical lattices *Phys. Rev.* A **63** 033401
[24] Gross C and Bloch I 2017 Quantum simulations with ultracold atoms in optical lattices *Science* **357** 995–1001
[25] Pezzè L, Smerzi A, Oberthaler M K, Schmied R and Treutlein P 2018 Quantum metrology with nonclassical states of atomic ensembles *Rev. Mod. Phys.* **90** 035005
[26] Hosten O, Engelsen N J, Krishnakumar R and Kasevich M A 2016 Measurement noise 100 times lower than the quantum-projection limit using entangled atoms *Nature* **529** 505–8
[27] Colombo S, Pedrozo-Peñafiel E, Adiyatullin A F, Li Z, Mendez E, Shu C and Vuletic V 2021 Time-reversal-based quantum metrology with many-body entangled states (arXiv:2106.03754)
[28] Isaev T A, Hoekstra S and Berger R 2010 Laser-cooled RaF as a promising candidate to measure molecular parity violation *Phys. Rev.* A **82** 052521
[29] Kudashov A D, Petrov A N, Skripnikov L V, Mosyagin N S, Isaev T A, Berger R and Titov A V 2014 *Ab initio* study of radium monofluoride (RaF) as a candidate to search for parity-and time-and-parity–violation effects *Phys. Rev.* A **90** 052513
[30] De Marco L, Valtolina G, Matsuda K, Tobias W G, Covey J P and Ye J 2019 A degenerate Fermi gas of polar molecules *Science* **363** 853–6
[31] Meyer E R and Bohn J L 2009 Electron electric-dipole-moment searches based on alkali-metal- or alkaline-earth-metal-bearing molecules *Phys. Rev.* A **80** 042508
[32] Andreev V *et al* (ACME Collaboration) 2018 Improved limit on the electric dipole moment of the electron *Nature* **562** 355
[33] Sandars P G H 1966 Enhancement factor for the electric dipole moment of the valence electron in an alkali atom *Phys. Lett.* **22** 290–1
[34] Bouchiat M A and Bouchiat C 1974 I. Parity violation induced by weak neutral currents in atomic physics *J. Phys.* **35** 899–927
[35] Flambaum V V and Khriplovich I B 1985 New bounds on the electric dipole moment of the electron and on *T*-odd electron–nucleon coupling *Sov. Phys. JETP* **62** 872
[36] Sunaga A, Abe M, Hada M and Das B P 2019 Merits of heavy–heavy diatomic molecules for electron electric-dipole-moment searches *Phys. Rev.* A **99** 062506
[37] Fleig T and DeMille D 2018 Breaching $d_e = 10^{-32}$ ecm with ultracold AgRa Searching for New Physics with Cold and Controlled Molecules Mainz, Germany https://dirac.ups-tlse.fr/fleig/talks/Fleig_Mainz2019.pdf.
[38] Guest J R, Scielzo N D, Ahmad I, Bailey K, Greene J P, Holt R J, Lu Z-T, O'Connor T P and Potterveld D H 2007 Laser trapping of Ra-225 and Ra-226 with repumping by room-temperature blackbody radiation *Phys. Rev. Lett.* **98** 093001
[39] Uhlenberg G, Dirscherl J and Walther H 2000 Magneto-optical trapping of silver atoms *Phys. Rev.* A **62** 063404
[40] Bilodeau R C, Scheer M and Haugen H K 1998 Infrared laser photodetachment of transition metal negative ions: studies on Cr^-, Mo^-, Cu^-, and Ag^- *J. Phys. B: At. Mol. Opt. Phys.* **31** 3885
[41] Andersen T, Haugen H K and Hotop H 1999 Binding energies in atomic negative ions: III *J. Phys. Chem. Ref. Data* **28** 1511
[42] Lim I S and Schwerdtfeger P 2004 Four-component and scalar relativistic Douglas–Kroll calculations for static dipole polarizabilities of the alkaline-earth-metal elements and their ions from Ca^n to Ra^n ($n = 0, +1, +2$) *Phys. Rev.* A **70** 062501
[43] Bast R, Heßelmann A, Sałek P, Helgaker T and Saue T 2008 Static and frequency-dependent dipole–dipole polarizabilities of all closed-shell atoms up to radium: a four-component relativistic DFT study *Comput. Phys. Commun.* **9** 445
[44] Hinds E A 1997 Testing time reversal symmetry using molecules *Phys. Scr.* **T70** 34
[45] Śmiałkowski M and Tomza M 2021 Highly polar molecules consisting of a copper or silver atom interacting with an alkali-metal or alkaline-earth-metal atom *Phys. Rev.* A **103** 022802
[46] Fleig T, Grasdijk O and DeMille D 2021 Using ultracold assembled AgRa molecules to search for time-reversal violation (in preparation)
[47] Fleig T, Olsen J and Marian C M 2001 The generalized active space concept for the relativistic treatment of electron correlation: I. Kramers-restricted two-component configuration interaction *J. Chem. Phys.* **114** 4775
[48] Fleig T, Olsen J and Visscher L 2003 The generalized active space concept for the relativistic treatment of electron correlation. II. Large-scale configuration interaction implementation based on relativistic 2- and 4-spinors and its application *J. Chem. Phys.* **119** 2963
[49] Knecht S, Jensen H J A and Fleig T 2010 Large-scale parallel configuration interaction. II. Two- and four-component double-group general active space implementation with application to BiH *J. Chem. Phys.* **132** 014108
[50] Knecht S 2009 Parallel relativistic multiconfiguration methods: new powerful tools for heavy-element electronic-structure studies *PhD Dissertation* Heinrich-Heine-Universität Düsseldorf, Düsseldorf, Germany
[51] Saue T *et al* 2020 The Dirac code for relativistic molecular calculations *J. Chem. Phys.* **152** 204104

[52] Lindroth E, Lynn B W and Sandars P G H 1989 Order α^2 theory of the atomic electric dipole moment due to an electric dipole moment on the electron *J. Phys. B: At. Mol. Opt. Phys.* **22** 559

[53] Fleig T and Nayak M K 2013 Electron electric-dipole-moment interaction constant for HfF^+ from relativistic correlated all-electron theory *Phys. Rev.* A **88** 032514

[54] Khriplovich I B and Lamoreaux S K 1997 *CP Violation Without Strangeness* (Berlin: Springer)

[55] Denis M, Nørby M S, Jensen H J A, Gomes A S P, Nayak M K, Knecht S and Fleig T 2015 Theoretical study on ThF^+, a prospective system in search of time-reversal violation *New J. Phys.* **17** 043005

[56] Fleig T, Nayak M K and Kozlov M G 2016 TaN, a molecular system for probing *P, T*-violating hadron physics *Phys. Rev.* A **93** 012505

[57] Dyall K G 2009 Relativistic double-zeta, triple-zeta, and quadruple-zeta basis sets for the 4*s*, 5*s*, 6*s*, and 7*s* elements *J. Phys. Chem.* A **113** 12638

[58] Dyall K G 2007 Relativistic double-zeta, triple-zeta, and quadruple-zeta basis sets for the 4*d* elements Y-Cd *Theor. Chem. Acc.* **117** 483

[59] Dyall K G 2012 Core correlating basis functions for elements 31–18 *Theor. Chem. Acc.* **131** 1217

[60] Pritchard B P, Altarawy D, Didier B, Gibson T D and Windus T L 2019 New basis set exchange: an open, up-to-date resource for the molecular sciences community *J. Chem. Inf. Model.* **59** 4814

[61] Fleig T, Jensen H J A, Olsen J and Visscher L 2006 The generalized active space concept for the relativistic treatment of electron correlation: III. Large-scale configuration interaction and multiconfiguration self-consistent-field four-component methods with application to UO_2 *J. Chem. Phys.* **124** 104106

[62] Olsen J 2000 The initial implementation and applications of a general active space coupled cluster method *J. Chem. Phys.* **113** 7140

[63] Huang W J, Wang M, Kondev F G, Audi G and Naimi S 2020 The AME 2020 atomic mass evaluation: I. Evaluation of input data, and adjustment procedures *Chin. Phys.* C **45** 030002

[64] Dzuba V A, Flambaum V V and Harabati C 2011 Relations between matrix elements of different weak interactions and interpretation of the parity-nonconserving and electron electric-dipole-moment measurements in atoms and molecules *Phys. Rev.* A **84** 052108 (erratum)
Dzuba V A, Flambaum V V and Harabati C 2012 Relations between matrix elements of different weak interactions and interpretation of the parity-nonconserving and electron electric-dipole-moment measurements in atoms and molecules *Phys. Rev.* A **85** 029901

[65] Fleig T and Jung M 2021 *PT*-odd interactions in atomic ^{129}Xe and phenomenological applications *Phys. Rev.* A **103** 012807

[66] Fleig T and Skripnikov L V 2020 *P, T*-violating and magnetic hyperfine interactions in atomic thallium *Symmetry* **12** 498

[67] Haeffler G, Hanstorp D, Kiyan I, Klinkmüller A E, Ljungblad U and Pegg D J 1996 Electron affinity of Li: a state-selective measurement *Phys. Rev.* A **53** 4127

[68] Hotop H and Lineberger W C 1985 Binding energies in atomic negative ions: II *J. Phys. Chem. Ref. Data* **14** 731

[69] Andersson K T, Sandstrom J, Kiyan I Y, Hanstorp D and Pegg D J 2000 Measurement of the electron affinity of potassium *Phys. Rev.* A **62** 022503

[70] Frey P, Breyer F and Holop H 1978 High resolution photodetachment from the rubidium negative ion around the Rb($5p_{1/2}$) threshold *J. Phys. B: At. Mol. Phys.* **11** L589–94

[71] Scheer M, Thøgersen J, Bilodeau R C, Brodie C A, Haugen H K, Andersen H H, Kristensen P and Andersen T 1998 Experimental evidence that the $6s6p^3P_j$ states of Cs^- are shape resonances *Phys. Rev. Lett.* **80** 684

[72] Landau A, Eliav E, Ishikawa Y and Kaldor U 2001 Benchmark calculations of electron affinities of the alkali atoms sodium to eka-francium (element 119) *J. Chem. Phys.* **115** 2389

[73] Kramida A, Ralchenko Y and Reader J (NIST ASD Team) 2020 NIST Atomic Spectra Database (Version 5.8) (Gaithersburg, MDNational Institute of Standards and Technology) available: https://physics.nist.gov/asd

[74] Dzuba V A, Allehabi S O, Flambaum V V, Li J and Schiller S 2021 Time keeping and searching for new physics using metastable states of Cu, Ag, and Au *Phys. Rev.* A **103** 022822

[75] Devlin J A and Tarbutt M R 2016 Three-dimensional Doppler, polarization-gradient, and magneto-optical forces for atoms and molecules with dark states *New J. Phys.* **18** 123017

[76] Devolder A, Desouter-Lecomte M, Atabek O, Luc-Koenig E and Olivier D 2021 Laser control of ultracold molecule formation: the case of RbSr *Phys. Rev.* A **103** 033301

[77] Devolder A, Luc-Koenig E, Atabek O, Desouter-Lecomte M and Dulieu O 2018 Proposal for the formation of ultracold deeply bound RbSr dipolar molecules by all-optical methods *Phys. Rev.* A **98** 053411

[78] Żuchowsky P S, Aldegunde J and Hutson J M 2010 Ultracold RbSr molecules can Be formed by magnetoassociation *Phys. Rev. Lett.* **105** 153201

[79] Brue D A and Hutson J M 2012 Magnetically tunable Feshbach resonances in ultracold Li–Yb mixtures *Phys. Rev. Lett.* **108** 043201

[80] Guttridge A, Hopkins S A, Frye M D, McFerran J J, JeremyHutson M and Cornish S L 2018 Production of ultracold Cs^* Yb molecules by photoassociation *Phys. Rev.* A **97** 063414

[81] Barbé V, Ciamei A, Pasquiou B, Reichsöllner L, Schreck F, Żuchowski P S and Hutson J M 2018 Observation of Feshbach resonances between alkali and closed-shell atoms *Nat. Phys.* **14** 881–4

[82] Green A, Li H, Toh J H S, Tang X, McCormick K C, Li M, Tiesinga E, Kotochigova S and Gupta S 2020 Feshbach resonances in p-wave three-body recombination within fermi-fermi mixtures of open-shell Li6 and closed-shell Yb173 atoms *Phys. Rev.* X **10** 031037

[83] Guttridge A, Frye M D, Yang B C, Hutson J M and Cornish S L 2018 Two-photon photoassociation spectroscopy of CsYb: ground-state interaction potential and interspecies scattering lengths *Phys. Rev.* A **98** 022707

[84] Köhler T, Góral K and Julienne P S 2006 Production of cold molecules via magnetically tunable Feshbach resonances *Rev. Mod. Phys.* **78** 1311

[85] Stellmer S, Pasquiou B, Grimm R and Schreck F 2012 Creation of ultracold Sr_2 molecules in the electronic ground state *Phys. Rev. Lett.* **109** 115302

[86] Ciamei A, Bayerle A, Chen C-C, Pasquiou B and Schreck F 2017 Efficient production of long-lived ultracold Sr2 molecules *Phys. Rev.* A **96** 013406

[87] Vitanov N V, Rangelov A A, Shore B W and Bergmann K 2017 Stimulated Raman adiabatic passage in physics, chemistry, and beyond *Rev. Mod. Phys.* **89** 015006